Cerenkov Luminescence Endoscopy: Improved Molecular Sensitivity with β^--Emitting Radiotracers

Colin M. Carpenter*[1], Xiaowei Ma*[2,3], Hongguang Liu[2], Conroy Sun[1], Guillem Pratx[1], Jing Wang[3], Sanjiv S. Gambhir[2], Lei Xing[1], and Zhen Cheng[2]

[1]Department of Radiation Oncology, Stanford University, Stanford, California; [2]Canary Center at Stanford for Cancer Early Detection, Molecular Imaging Program at Stanford (MIPS), Department of Radiology and Bio-X Program, Stanford University, Stanford, California; and [3]Department of Nuclear Medicine, Xijing Hospital, Fourth Military Medical University, Xi'an, Shaanxi, China

Cerenkov luminescence endoscopy (CLE) is an optical technique that captures the Cerenkov photons emitted from highly energetic moving charged particles (β^+ or β^-) and can be used to monitor the distribution of many clinically available radioactive probes. A main limitation of CLE is its limited sensitivity to small concentrations of radiotracer, especially when used with a light guide. We investigated the improvement in the sensitivity of CLE brought about by using a β^- radiotracer that improved Cerenkov signal due to both higher β-particle energy and lower γ noise in the imaging optics because of the lack of positron annihilation. **Methods:** The signal-to-noise ratio (SNR) of ^{90}Y was compared with that of ^{18}F in both phantoms and small-animal tumor models. Sensitivity and noise characteristics were demonstrated using vials of activity both at the surface and beneath 1 cm of tissue. Rodent U87MG glioma xenograft models were imaged with radiotracers bound to arginine-glycine-aspartate (RGD) peptides to determine the SNR. **Results:** γ noise from ^{18}F was demonstrated by both an observed blurring across the field of view and a more pronounced fall-off with distance. A decreased γ background and increased energy of the β particles resulted in a 207-fold improvement in the sensitivity of ^{90}Y compared with ^{18}F in phantoms. ^{90}Y-bound RGD peptide produced a higher tumor-to-background SNR than ^{18}F in a mouse model. **Conclusion:** The use of ^{90}Y for Cerenkov endoscopic imaging enabled superior results compared with an ^{18}F radiotracer.

Key Words: Cerenkov luminescence endoscopy; Cerenkov luminescence imaging; radionuclides; β-emitter

J Nucl Med 2014; 55:1905–1909
DOI: 10.2967/jnumed.114.139105

Molecular imaging is at the center of the current explosion in the understanding of biology and disease in living systems. Bioluminescence (*1*), fluorescence (*2,3*), and nuclear imaging paradigms (*4,5*) in particular have enabled noninvasive investigation of gene or protein expression during disease progression and after treatment perturbations. The opportunity to use an optical imaging system for nuclear agents in addition to bioluminescence and fluorescence has ignited interest in Cerenkov luminescence imaging (CLI) (*6*), because lower-cost systems may be constructed that enable more researchers to perform molecular imaging without a significant investment. Potentially equally advantageous is that radiotracers can be imaged with conventional medical optics, such as endoscopes, laparoscopes, and fibers (*7*).

CLI provides a means to image nuclear tracers by recording the Cerenkov photons that are emitted from highly energetic charged particles that move more quickly than the relativistic speed of light in the medium (*8–11*). CLI has been verified for monitoring a variety of molecular targets and cancer treatment efficacy by numerous investigators (*12–16*), and recently CLI has also been demonstrated in pilot cases to identify thyroid and lymph nodes in the clinic (*17,18*).

One of the main drawbacks of CLI is its poor sensitivity due to the relatively low number of optical photons emitted per charged particle (*11*) and the concomitant absorption and scatter of tissue that is especially high in the Cerenkov light spectrum. This disadvantage often demands long camera integration times, high-activity injections, or subsurface imaging for feasible image signal-to-noise ratio (SNR). One method to circumvent this challenge is the use of additional imaging probes that down-convert Cerenkov light to longer-wavelength photons that have a lower absorption and scatter. Liu et al. demonstrated this technique using quantum dots coinjected with ^{131}I to produce 655- to 800-nm emissions, depending on the quantum dots used (*19*). Dothager et al. (*20*) and Sun et al. (*21*) showed similar performance using quantum dots and a phosphor nanoparticle, respectively, to down-convert Cerenkov and charged particle emissions to near-infrared light. However, these methods require additional dyes or particles, with their own associated challenges of delivery, biocompatibility, quality control, and efficiency.

Another means to overcome the limit of sensitivity in radiologic Cerenkov imaging is the use of more highly energetic radiotracers. Numerous investigators have demonstrated the increased light output per nuclear decay that results from using more energetic radionuclides such as ^{90}Y (2.28 MeV, 100%) and ^{32}P (1.71 MeV, 100%) (*10,22*). In this communication, we demonstrate a dramatic improvement in signal sensitivity that may be provided by β^--emitting radioisotopes such as ^{90}Y, versus β^+-emitting radioisotopes such as ^{18}F, when using fiber light guides for imaging.

Received Feb. 23, 2014; revision accepted Aug. 20, 2014.
For correspondence or reprints contact either of the following:
Zhen Cheng, Department of Radiology, Stanford University, 1201 Welch Rd., Lucas Expansion, P095, Stanford, CA 94305.
E-mail: zcheng@stanford.edu
Lei Xing, Department of Radiation Oncology, Stanford University School of Medicine, 875 Blake Wilbur Dr., Stanford, CA 94305-5847.
E-mail: lei@stanford.edu
*Contributed equally to this work.
Published online Oct. 9, 2014.

This decreased sensitivity is demonstrated to arise from the increased noise created in the optical instrumentation by 511-keV γ particles produced during positron annihilation of β^+-emitting radioisotopes. This background signal, caused by both Cerenkov and scintillation events, degrades sensitivity and thus SNR. This noise is shown to affect signal by 1 order of magnitude and is dependent on the optical instrumentation in the system. Taken together, we show that the gains from a more highly energetic charged particle, and the lack of positron emission from ^{90}Y, result in a 207-fold increase in sensitivity. These advantages are demonstrated via imaging through a phantom of simulated tissue and in a mouse model in vivo.

MATERIALS AND METHODS

Cerenkov Luminescence Endoscopy (CLE)

A custom-built flexible fiber Cerenkov luminescence endoscope (*7*) was used for all studies. Briefly, a compact camera lens (F/1.4, 12 mm; Schneider) was coupled to the distal end of a coherent imaging fiber bundle (IG154; Schott); the imaging fiber was coupled through relay optics to a single-photon imaging camera (I-CCD [Stanford Photonics Inc.] or EM-CCD [Princeton Instruments]). This setup was placed in a black box to minimize background light and to emulate a light-tight anatomic cavity. Images were processed after the initial acquisition using software thresholding to remove low-intensity pixels (corresponding to thermal and read noise on the charge-coupled device) and cosmic events and subsequently were stored. Subjects were placed on a motorized platform that could be adjusted to focus the imaging system.

Radiotracer Cerenkov Imaging Agents

All chemicals obtained commercially were of analytic grade (Sigma-Aldrich). Radiotracers were transferred and handled according to institutional guidelines. A polyethylene glycol (PEG)–modified dimer RGD (PRGD2) was labeled by 4-nitrophenyl 2-^{18}F-fluoropropionate (^{18}F-NFP) to synthesize the ^{18}F-FP-PRGD2 as previously described (*23*). $^{90}YCl_3$ was purchased from Perkin Elmer. DOTA-$PRGD_2$ was synthesized by conjugation of DOTA mono-*N*-hydroxysuccinimide ester with $PRGD_2$ and characterized by matrix-assisted laser desorption–ionization time-of-flight mass spectrometry. The measured molecular weight was 1,925.16, and the expected molecular weight ($[M + H]^+$) was 1,926.08. For ^{90}Y-$PRGD_2$ synthesis, 20 μg of DOTA-$PRGD_2$ and 0.3 mg of sodium ascorbate dissolved in 200 μL of 0.1 M ammonium acetate buffer (pH 5.5) were added to 100 μL of $^{90}YCl_3$ stock solution (37 MBq [1 mCi]) in 0.1 M ammonium acetate buffer (pH 5.5). The reaction mixture was then heated at 95°C for 30 min. The solution was diluted with 300 μL of 0.05 M ethylenediaminetetraacetic acid and then analyzed and purified with a radio–high-performance liquid chromatography. The mobile phase started with 95% solvent A (distilled water) and 5% solvent B (acetonitrile) and continued to 5% solvent A and 95% solvent B at 30 min. The eluted fraction containing ^{90}Y-$PRGD_2$ (retention time, 16.8 min) was collected and dried using an evaporator. The purity of the product analyzed with high-performance liquid chromatography was higher than 95%.

Phantom Experiments

A series of phantom experiments was performed to characterize the sensitivity and noise of the CLE system for imaging ^{90}Y- and ^{18}F-labeled tracers. To determine the sensitivity for ^{90}Y, three 0.2-mL polymerase chain reaction vials with 10 μL of known concentrations of ^{90}Y (0.3, 3, and 37 kBq [0.008, 0.08, and 1 μCi, respectively]) were imaged over 5 min with the CLE system placed about 8 cm from the samples. To determine the sensitivity for ^{18}F, 1 vial of ^{18}F (3.7 MBq [100 μCi]) was placed in the imaging chamber and imaged over the course of decay (19 h 43 min, or ~10 half-lives) using successive 5-min integration periods. To determine cross-section noise profiles, equivalent volumes of radiotracer were next placed underneath 1 cm of chicken breast. To determine noise as a function of subject-to-optic distance, vials of ^{18}F and ^{90}Y were imaged at varying distances from the distal end of the imaging fiber, from 12.5 to 75 mm.

Three sets of regions of interest (ROIs) were generated from the CLE images to compare the SNR and noise characteristics of the Cerenkov signal generated from ^{18}F and ^{90}Y. Contrast agent ROIs were determined by manual selection of the region of activity as determined by white-light reflectance imaging. Background ROIs were determined by manually selecting a region immediately outside the activity/contrast agent ROI. Zero-signal ROIs were generated by sampling the region of the charge-coupled device that was outside the projected image from the proximal end of the imaging fiber (available because the image produced by the fiber did not entirely fill the active area of the charge-coupled device). SNR was determined by calculating the ratio between the zero-signal ROI subtracted from the contrast-signal ROI and the zero-signal ROI subtracted from the background ROI.

The Frank–Tamm formula describes Cerenkov photon production, which increases as the β-particle energy increases. Because higher-energy charged particles create more Cerenkov emission than lower-energy charged particles, the Frank–Tamm formula was used to correct for the increase in Cerenkov signal (*9*) due to the higher-energy charged particle emitted by ^{90}Y.

Tumor Model and Rodent Preparation

The animal procedures were performed according to a protocol approved by the Stanford University Institutional Animal Care and Use Committee. U87MG glioma cells were cultured in Dulbecco modified Eagle medium supplemented with 10% fetal bovine serum and 1% penicillin/streptomycin (Invitrogen Life Technologies). The cell line was maintained in a humidified atmosphere of 5% CO_2 at 37°C, with the medium changed every other day. A 75% confluent monolayer was detached with trypsin and dissociated into a single-cell suspension for further cell culture. Approximately 1×10^6 U87MG cells suspended in 50 μL of phosphate-buffered saline (0.1 M, pH 7.2; Invitrogen) were implanted subcutaneously in the flanks of nude mice. Tumors were allowed to grow to a size of 150–200 mm^3 (2–3 wk).

In Vivo Animal Imaging

Images were acquired on imaging days 1 (^{18}F-FP-$PRGD_2$) and 3 (^{90}Y-$PRGD_2$). On day 1, 4 mice were anesthetized with an isoflurane vaporizer (SAS3-EVAC4; Molecular Imaging Products Co.) and subsequently injected via the tail vein with about 33 MBq (900 μCi) of ^{18}F-FP-$PRGD_2$. After about 90 min (86, 91, 95, and 87 min for mice 1, 2, 3, and 4, respectively), uptake of ^{18}F-FP-$PRGD_2$ was verified by an IVIS imaging system (Perkin-Elmer); the mice were then immediately imaged with the CLE system to determine tissue uptake of ^{18}F-FP-$PRGD_2$. On day 3, each of the 4 mice was anesthetized and injected via the tail vein with 8.1 MBq (220 μCi) of ^{90}Y-$PRGD_2$. After about 90 min, the tracer uptake in the mice was verified by an IVIS system; they were subsequently imaged with the CLE system to determine ^{90}Y-$PRGD_2$ uptake. Signal from within tumor ROIs (identified as the bulk of tissue under ambient-light illumination), integrated over 6 min, was compared with signal background outside the tumor regions (tissue on the hind leg identified under ambient illumination) for both radiotracers. After imaging, all mice were sacrificed to harvest tumors and organs of interest; these tissues were weighed wet and measured with a γ counter (corrected for half-life and particle energy). Radioactivity uptake was expressed as a percentage of the injected radioactive dose per gram of tissue.

RESULTS

Sensitivity Comparison

Figure 1A shows the signal of varying activities of ^{90}Y and ^{18}F, with each time point comprising 5 min of signal integration. Using an SNR of 10 to define the noise floor, the ^{90}Y minimum detectable activity was 0.056 μCi (2.1 kBq); the minimum detectable activity for ^{18}F was 11.63 μCi (430.3 kBq). These data demonstrate a 207-fold improvement in SNR for ^{90}Y compared with ^{18}F, when controlled for activity.

Radiotracer Noise Comparison

Cerenkov SNRs from ^{90}Y and ^{18}F were compared and normalized for the energy of the charged particle (positron and electron, respectively), to compare the impact of fiber noise on SNR. Figure 1B shows the signal difference between ^{18}F and ^{90}Y after controlling for the higher light output in ^{90}Y due to the higher energy of the ^{90}Y charged particle. A 5.1-fold gain in SNR is shown between radionuclides when controlled for the increased light output of ^{90}Y due to its increased β energy. This improved signal in the case of ^{90}Y imaging is caused by the lack of the γ photon, which creates noise in the imaging optics because of Cerenkov and scintillating events in the light guide.

As further evidence of the effect of decreased SNR due to the γ noise present in positron emission, the spatial extent of the increase in noise created in the optics is shown in Figure 2. Radiotracers were placed underneath a 1-cm-thick piece of chicken breast to simulate the propagation of Cerenkov light through tissue. Figures 2A and 2B show the Cerenkov light emitted by a vial of ^{18}F radionuclide through chicken breast and overlaid on a white-light image of the chicken breast. Figures 2C and 2D show the Cerenkov light emitted by a vial of ^{90}Y radionuclide through chicken breast and overlaid on a white-light image of the chicken breast. The volume of activity was equivalent for both radiotracers. Figure 2E shows spatial signal fall-off across the camera for both ^{18}F and ^{90}Y. It is apparent that although the vial is confined to a small region of tissue, the signal is blurred across the camera when imaging with ^{18}F but is more localized around the ^{90}Y vial. More specifically, the full width at half maximum for the ^{18}F is 3.2-fold larger in spatial extent than that for ^{90}Y because of the γ noise in the imaging fiber bundle in ^{18}F.

Figure 2F shows the effect of varying distance from the distal-end imaging fiber to the vials of radionuclide. With ^{18}F, the production of 511-keV γ photons generates background noise in the fiber; this signal falls off quadratically with distance, as expected. The background noise generated in the fiber has 32% greater signal than the zero-signal region (the region of the charge-coupled device where the image does not project). In contrast, the fiber background using ^{90}Y radiotracer results in negligible background fiber noise variation with distance; the relative background noise generated in the fiber is just 2% higher than the zero-signal region. This phenomenon is consistent with a lack of γ-photon noise with ^{90}Y. Thus, the use of ^{18}F results in a relative 16-fold (32%/2%) increase in background noise compared with imaging CLE with ^{90}Y.

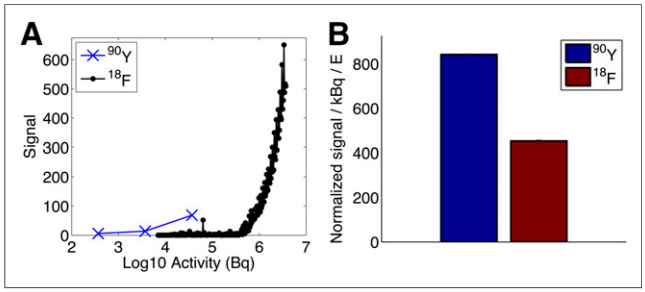

FIGURE 1. (A) Sensitivity comparison between ^{18}F and ^{90}Y. (B) Comparison between tracer SNR normalized for activity and light output, which is dependent on charged-particle energy.

Investigation in a Small-Animal Model

To compare CLE in vivo with ^{90}Y versus ^{18}F, an experiment was performed with the U87MG tumor mouse model and the radiolabeled PRGD$_2$. Both ^{18}F and ^{90}Y radionuclides were labeled with arginine-glycine-aspartate (RGD) peptides, which target the $\alpha_v\beta_3$ integrins in the tumor vasculature and tissue. Four mice with tumors on the flanks were imaged after the tumors had grown larger than 150–200 mm^3. On experiment day 1, the mice were injected with ^{18}F-FP-PRGD$_2$ via the tail vein and imaged using the CLE system after 90 min of uptake. Results are shown for an example mouse in Figure 3D, and the ambient-light overlay is shown in Figure 3E. On day 3, the 4 mice were then injected with ^{90}Y-PRGD$_2$ and imaged at 90 min by CLE, as shown in Figure 3F; the ambient-light overlay is shown in Figure 3G. After imaging with CLE, all mice were sacrificed for ^{90}Y-PRGD$_2$ biodistribution studies; the results comparing peptide biodistribution with ^{18}F-FP-PRGD$_2$ at 90 min, which was retrieved from Liu et al. (*24*), are shown in Figures 3A and 3B. This comparison shows no significant difference in the mean tumor-to-muscle uptake ratio between the probes (both are about 14×), demonstrating no difference in affinity for ^{90}Y-PRGD$_2$ versus ^{18}F-FP-PRGD$_2$.

Compared with the biodistribution data, the CLE imaging has lower observed tumor-to-background contrast. However, contrast recovery is better with ^{90}Y-PRGD$_2$ than with ^{18}F-FP-PRGD$_2$. Tumor-to-background ratios between tumor tissue in the flanks and nontumor tissue outside the xenograft tumor region were compared for the 2 tracers. Both tracers showed tumor-to-background contrast above the noise floor. Figure 3C shows that the mean tumor-to-background ratio was 1.1 ± 0.1 for ^{18}F-FP-PRGD$_2$ for the 4 mice. In contrast, the mean tumor-to-background ratio for ^{90}Y-PRGD$_2$ was 3.4 ± 2.0. Thus, contrast was significantly greater for ^{90}Y radiotracer than for ^{18}F ($P = 0.035$, 1-sided paired t test, MATLAB). Thus, the recovered CLE contrast of ^{90}Y-PRGD$_2$ was not due to the affinity of peptides but to the improved performance of CLE with a β-emitting tracer.

DISCUSSION

Although there are many enticing applications for the use of Cerenkov light in molecular imaging, poor sensitivity is the key challenge. This poor sensitivity demands that higher activities, shallower ROIs, and more sensitive optics be used. In this study, we demonstrated the advantages of Cerenkov imaging with ^{90}Y. To date, most of the literature on Cerenkov light has investigated imaging the ^{18}F radiotracer. Although imaging ^{18}F-FDG provides for the use of a Food and Drug Administration–cleared contrast agent with decades of clinical experience, there are distinct disadvantages to using radiotracers containing the ^{18}F nuclide, as demonstrated in our study.

One disadvantage with ^{18}F is that less than 100% of the radioactive decay of ^{18}F is due to the Cerenkov-producing positron emission (96.9%), versus 100% β^- emission for ^{90}Y. A second, even worse, disadvantage is that ^{18}F has low charged-particle energy. The average energy of an emitted charged particle is 250 keV (*25*), which is below the Cerenkov limit of 263 keV in

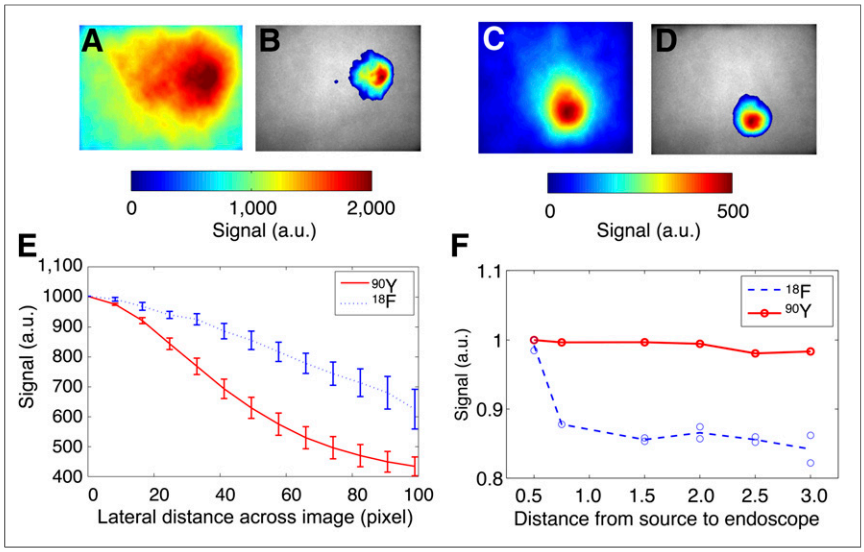

FIGURE 2. (A and B) CLE emission (A) and CLE overlay (B) over ambient-light image of ^{18}F vial covered with 1 cm of chicken breast. (C and D) CLE emission (C) and CLE overlay (D) over ambient-light image of ^{90}Y vial covered with 1 cm of chicken breast. (E) Cross-sectional plot of line response of signal across 1 row of imaging fiber bundle, with 0 defined as optical axis. (F) Background noise (region outside vial containing radiotracer) in imaging fiber bundle vs. distance from vial to endoscope (in inches). a.u. = arbitrary units.

tissue (water) (*11*). On the other hand, the average energy of an emitted charged particle from ^{90}Y is 934 keV, and 90% of the emissions are beyond the Cerenkov threshold. This advantage provides a 40-fold improvement in light output (*11*). A third disadvantage, which is a main focus of this study, is the noise created in the imaging optics caused by the γ-photon emission of ^{18}F.

The decay of positrons to 511-keV γ photons caused by positron annihilation results in the generation of Cerenkov events in the camera optics and, if present, imaging fiber optics. The detection of γ photons emitted by ^{18}F-FDG is used by the many γ probes that have been studied in the past to confirm preoperative ^{18}F-FDG localization in tumors of the head and neck (*26*), lung (*27*), large bowel, ovary (*28*), and other sites. These γ probes typically use a scintillator coupled to a sensitive detector, such as a photomultiplier tube. In the case of the CLE system, the fiber light guide acts as the scintillator. Cerenkov and scintillation light caused by excitation of impurities in the optical fibers lead to a low-frequency signal bias that presents in the camera. This source of noise is difficult to isolate because it is created in the path between the entrance pupil and the camera. Although this experiment was designed to realistically model the interaction of γ-photon emissions with the fiber optics, the amount of background noise depends on the optical system and the distance from the activity. With a positron emitter, noise will cause a loss in sensitivity in applications that position a light guide in a body cavity, because of increased nonspecific background uptake of ^{18}F-FDG. In these cases, alternative methods to reduce noise, such as by recording background uptake with an independent γ probe, may help subtract out some of the noise, as long as the detector has a sufficient dynamic range. As we have argued in this study, a superior choice would be the use of ^{90}Y, since it does not generate the 511-keV photons and would result in even greater sensitivity than the surface imaging studied here. Meanwhile, the higher yield of Cerenkov radiation from ^{90}Y will decrease the injected dose of this radionuclide-based probe used for imaging in detection and tumor therapy. The radiation dose used in therapy is absolutely enough for such highly sensitive CLE imaging. Here, for imaging we used ^{90}Y in only a very small amount, which would not be expected to cause radiation injury to normal tissue.

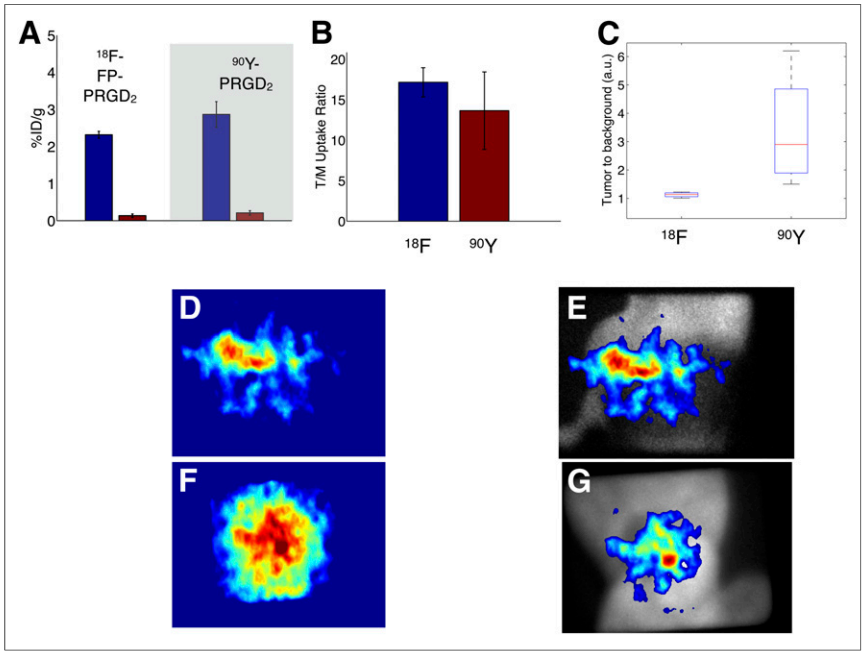

FIGURE 3. In vivo comparison of CLE improvement using ^{90}Y-PRGD$_2$ vs. ^{18}F-FP-PRGD$_2$. (A and B) Biodistribution results comparing tumor and muscle (A) and tumor-to-muscle (T/M) ratio (B) for both peptides. (C) Tumor-to-background ratio from ^{90}Y-PRGD$_2$ vs. ^{18}F-FP-PRGD$_2$ for all 4 mice as determined by CLE. (D and E) CLE image (D) and ambient-light overlay (E) of ^{90}Y-PRGD$_2$ emitted from mouse flank. (F and G) CLE image (F) and ambient-light overlay (G) of ^{18}F-FP-PRGD$_2$ emitted from mouse flank.

Although the use of ^{90}Y results in a significantly increased tumor-to-background ratio compared with the use of ^{18}F for CLE, there is a significant degradation in tumor-to-background (muscle) contrast when compared with the biodistribution data. This decrease in SNR is partially caused by the ROI selection: if the maximum signal in the tumor is compared with the background, the ^{90}Y-PRGD$_2$ ratio is 6.5 whereas the ^{18}F-FP-PRGD$_2$ ratio is 2.0. In comparison, use of the median of the ROI, as displayed in Figure 3B, results in some

partial-volume effects from the thinner edges of the tumor ROIs. A further confounder may arise from the oxygenation differences between tumor and muscle tissue. Because of the differing absorption spectra of oxy- and deoxyhemoglobin, which might be present in different concentrations in these tissues, the emitted Cerenkov light might consist of dissimilar wavelengths, which would undergo varied absorption when passing through the skin (*29*).

CONCLUSION

The performance of CLI may be poor because of the difficulty in detecting emissions from the tissue. For ^{18}F, the radioisotope that has been most commonly used to perform CLI experiments, both charged-particle mean energy and the presence of γ noise result in a 207-fold reduction in sensitivity compared with using ^{90}Y. This sensitivity loss may be even more severe in a body cavity and depends on the distance between the light guide and the radiation source, the mass of the light guide, and the material. The results observed in this work can also likely be extended to other β-emitting radionuclides. Thus, it is recommended that a pure β radionuclide such as ^{90}Y be used, if possible, for CLE.

DISCLOSURE

The costs of publication of this article were defrayed in part by the payment of page charges. Therefore, and solely to indicate this fact, this article is hereby marked "advertisement" in accordance with 18 USC section 1734. This work was supported in part by the Office of Science (BER), the U.S. Department of Energy (DE-SC0008397), the Key Program of the National Natural Science Foundation of China (grant 81230033), and Department of Defense Breast Cancer postdoctoral fellowships W81XWH-11-1-0087, W81XWH-11-1-0070, and W81XWH-10-1-0506. No other potential conflict of interest relevant to this article was reported.

REFERENCES

1. Contag CH, Jenkins D, Contag PR, Negrin RS. Use of reporter genes for optical measurements of neoplastic disease in vivo. *Neoplasia.* 2000;2:41–52.
2. Weissleder R, Tung CH, Mahmood U, Bogdanov JA. In vivo imaging of tumors with protease-activated near-infrared fluorescent probes. *Nat Biotechnol.* 1999;17:375–378.
3. Tyagi S, Bratu DP, Kramer FR. Multicolor molecular beacons for allele discrimination. *Nat Biotechnol.* 1998;16:49–53.
4. Tjuvajev JG, Stockhammer G, Desai R, et al. Imaging the expression of transfected genes in vivo. *Cancer Res.* 1995;55:6126–6132.
5. Gambhir SS, Barrio JR, Phelps ME, et al. Imaging adenoviral-directed reporter gene expression in living animals with positron emission tomography. *Proc Natl Acad Sci USA.* 1999;96:2333–2338.
6. Xu Y, Liu H, Cheng Z. Harnessing the power of radionuclides for optical imaging: Cerenkov luminescence imaging. *J Nucl Med.* 2011;52:2009–2018.
7. Liu H, Carpenter C, Jiang H, Pratx G, et al. Intraoperative imaging of tumors using Cerenkov luminescence endoscopy: a feasibility experimental study. *J Nucl Med.* 2012;53:1579–1584.
8. Robertson R, Germanos MS, Li C, Mitchell GS, Cherry SR, Silva MD. Optical imaging of Cerenkov light generation from positron-emitting radiotracers. *Phys Med Biol.* 2009;54:N355–N365.
9. Spinelli AE, D'Ambrosio D, Calderan L, Marengo M, Sbarbati A, Boschi F. Cerenkov radiation allows in vivo optical imaging of positron emitting radiotracers. *Phys Med Biol.* 2010;55:483–495.
10. Liu H, Ren G, Miao Z, et al. Molecular optical imaging with radioactive probes. *PLoS ONE.* 2010;5:e9470.
11. Mitchell GS, Gill RK, Boucher DL, Li C, Cherry SR. In vivo Cerenkov luminescence imaging: a new tool for molecular imaging. *Philos Transact A Math Phys Eng Sci.* 2011;369:4605–4619.
12. Natarajan A, Habte F, Liu H, et al. Evaluation of ^{89}Zr-rituximab tracer by Cerenkov luminescence imaging and correlation with PET in a humanized transgenic mouse model to image NHL. *Mol Imaging Biol.* 2013;15:468–475.
13. Ruggiero A, Holland JP, Lewis JS, Grimm J. Cerenkov luminescence imaging of medical isotopes. *J Nucl Med.* 2010;51:1123–1130.
14. Holland JP, Normand G, Ruggiero A, Lewis JS, Grimm J. Intraoperative imaging of positron emission tomographic radiotracers using Cerenkov luminescence emissions. *Mol Imaging.* 2011;10:177–186, 1–3.
15. Liu H, Ren G, Liu S, et al. Optical imaging of reporter gene expression using a positron-emission-tomography probe. *J Biomed Opt.* 2010;15:060505.
16. Xu Y, Liu H, Chang E, Jiang H, Cheng Z. Cerenkov luminescence imaging (CLI) for cancer therapy monitoring. *J Vis Exp.* 2012;(69):e4341.
17. Spinelli AE, Ferdeghini M, Cavedon C, et al. First human Cerenkography. *J Biomed Opt.* 2013;18:20502.
18. Thorek DLJ, Riedl CC, Grimm J. Clinical Cerenkov luminescence imaging of ^{18}F-FDG. *J Nucl Med.* 2014;55:95–98.
19. Liu H, Zhang X, Xing B, Han P, Gambhir SS, Cheng Z. Radiation-luminescence-excited quantum dots for in vivo multiplexed optical imaging. *Small.* 2010; 6:1087–1091.
20. Dothager RS, Goiffon RJ, Jackson E, Harpstrite S, Piwnica-Worms D. Cerenkov radiation energy transfer (CRET) imaging: a novel method for optical imaging of PET isotopes in biological systems. *PLoS ONE.* 2010;5:e13300.
21. Sun C, Carpenter C, Pratx G, Xing L. Facile synthesis of amine-functionalized Eu^{3+}-doped $La(OH)_3$ nanophosphors for bioimaging. *Nanoscale Res Lett.* 2011;6:24.
22. Park JC, Il An G, Park S, et al. Luminescence imaging using radionuclides: a potential application in molecular imaging. *Nucl Med Biol.* 2011; 38:321–329.
23. Chin FT, Shen B, Liu S, et al. First experience with clinical-grade ([^{18}F]FPP (RGD_2): an automated multi-step radiosynthesis for clinical PET studies. *Mol Imaging Biol.* 2012;14:88–95.
24. Liu S, Liu Z, Chen K, et al. ^{18}F-labeled galacto and PEGylated RGD dimers for PET imaging of αvβ3 integrin expression. *Mol Imaging Biol.* 2010;12: 530–538.
25. Levin CS, Hoffman EJ. Calculation of positron range and its effect on the fundamental limit of positron emission tomography system spatial resolution. *Phys Med Biol.* 1999;44:781–799.
26. Agrawal A, Hall NC, Ringel MD, Povoski SP, Martin EW Jr. Combined use of perioperative TSH-stimulated ^{18}F-FDG PET/CT imaging and gamma probe radioguided surgery to localize and verify resection of iodine scan-negative recurrent thyroid carcinoma. *Laryngoscope.* 2008;118:2190–2194.
27. Moffatt-Bruce SD, Povoski SP, Sharif S, et al. A novel approach to positron emission tomography in lung cancer. *Ann Thorac Surg.* 2008;86:1355–1357.
28. Cohn DE, Hall NC, Povoski SP, Seamon LG, Farrar WB, Martin EW Jr. Novel perioperative imaging with ^{18}F-FDG PET/CT and intraoperative ^{18}F-FDG detection using a handheld gamma probe in recurrent ovarian cancer. *Gynecol Oncol.* 2008;110:152–157.
29. Wilson BC, Jacques SL. Optical reflectance and transmittance of tissues: principles and applications. *IEEE J Quantum Electron.* 1990;26:2186–2199.